Journal of Alloys and Compounds 508 (2010) 141–146

Contents lists available at ScienceDirect

Journal of Alloys and Compounds

journal homepage: www.elsevier.com/locate/jallcom

Impedance spectroscopy and conductivity mechanism of $CoFe_2O_4$–$Pb(Zr_{0.53}Ti_{0.47})O_3$ composite thick films

W. Chen [a], W. Zhu [a,*], C. Ke [a], Z. Yang [a,b], L. Wang [b], X.F. Chen [a], O.K. Tan [a]

[a] Microelectronics Center, School of Electrical and Electronic Engineering, Nanyang Technological University, No. 50 Nanyang Avenue, Singapore 639798, Singapore
[b] Division of Physics and Applied Physics, School of Physical and Mathematical Science, Nanyang Technological University, Singapore 637371, Singapore

ARTICLE INFO

Article history:
Received 5 May 2010
Received in revised form 5 August 2010
Accepted 6 August 2010
Available online 18 August 2010

Keywords:
Multiferroic
Thick films
Sol–gel
Impedance
Conductivity

ABSTRACT

In the present work, the impedance spectroscopy and conductivity mechanism of multiferroic $CoFe_2O_4$–$Pb(Zr_{0.53}Ti_{0.47})O_3$ composite thick films have been investigated. Temperature dependent impedance spectroscopy analysis was conducted in the temperature range of 25–275 °C with the frequency ranging from 100 Hz to 1 MHz. Two impedance relaxation peaks were observed at high frequency with low temperature, and low frequency with high temperature. These peaks were attributed to grain and grain boundary effect, respectively. Electric modulus spectra clearly presented the contributions from both effects in terms of remarkably semicircle arcs. Two different grain boundary effects were reflected in the electric modulus spectra: one caused by homogeneous PZT grain boundary and the other due to the heterogeneous CFO and PZT grain boundary. The activation energy calculated from modulus spectra was consistent with the estimated value from impedance spectra. Investigation on dielectric spectra revealed a dc conductivity region and two nearly constant loss regions, corresponding to the grain effect and two different grain boundary effects, which were also demonstrated in ac conductivity spectra. Furthermore, ion hopping and transport mechanism were unveiled through the analysis on ac conductivity spectra.

1. Introduction

Multiferroic composites have drawn intensive interests in the past years due to the coexistence of ferroelectric and ferromagnetic ordering as well as the magnetoelectric coupling (ME) effect induced by both constituted phases [1–4]. Not only does the ME effect in these materials promise them a candidate for ME devices application [5], but these multiferroic materials could also be potentially used in devices which demand either ferroelectric or ferromagnetic properties, such as sensors, actuators and other devices which take advantage of ferroelectric and ferromagnetic properties simultaneously without their coupling properties [6–8]. Currently, a number of single phase materials with intrinsic ME effect have been found, but this effect in them is very weak [9,10]. In contrast, a much larger extrinsic ME effect can be realized in two-phase composites by means of strains transferring between a magnetostrictive phase and piezoelectric phase under their individual magnetic and electric fields [6,7]. So far, various methods have been developed to synthesize two-phase multiferroic thin films, thick films and bulk materials, especially on $CoFe_2O_4$–$Pb(Zr_{0.53}Ti_{0.47})O_3$ (CFO–PZT) system due to the large magnetostrictive coefficient of CFO and the promising piezoelectric coefficient of PZT [11–13]. However, a detailed dielectric study on this material has been lacking except for the recent reports on the multilayered CFO–PZT thin film and its bulk ceramics [13,14]. In our previous work, CFO–PZT composite thick films have been prepared and optimized, yielding promising ferromagnetic and ferroelectric properties [15,16]. In order to develop a deeper understanding of the CFO–PZT system, a detailed discussion on temperature and frequency dependent impedance spectroscopy was conducted and is the focus of this work.

CFO–PZT composite thick films were prepared on $Pt/TiO_2/SiO_2/Si$ substrate by a hybridized sol–gel processing and spin coating technique followed by the optimization of film compactness through PZT sol infiltration [15,16]. A high annealing temperature of 800 °C was then applied to achieve a high crystallinity. Subsequently, the phase structures and microstructures of the composite thick films were characterized by X-ray diffraction and scanning electron microscope. Lastly, temperature and frequency dependent impedance spectroscopy was carried out allowing for a detailed discussion of the physical mechanisms.

2. Experimental

The fabrication process of the CFO–PZT multiferroic composite thick films has been detailed elsewhere [15]. An anneal at 800 °C in a tube furnace under air ambient was applied to improve crystallinity of the composite thick films. The substrate was changed to $Pt/TiO_2/SiO_2/Si$ wafer from the $Pt/Ti/SiO_2/Si$ one used in the previ-

* Corresponding author.
E-mail address: ewgzhu@gmail.com (W. Zhu).

0925-8388/$ – see front matter
doi:10.1016/j.jallcom.2010.08.029

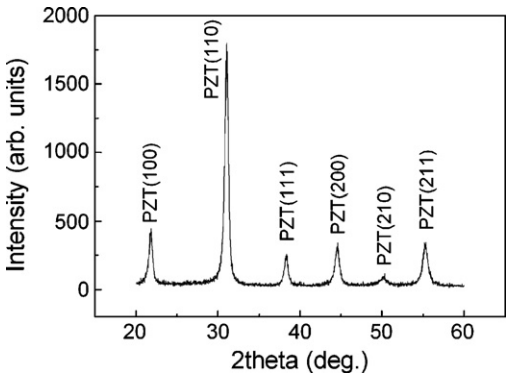

Fig. 1. X-ray diffraction pattern of the CFO–PZT composite thick film.

ous work [17]. Additionally, higher densification of the composite thick films was achieved by introducing sufficient sol infiltration in between slurry layers [16]. Phase structure of our composite thick films were performed on a Siemens D 5005 X-ray diffractometer (XRD) using CuK_α radiation ($\lambda = 1.5406$ Å) in a detector mode. Surface morphology and cross-sectional microstructure were observed using a scanning electron microscope (FE-SEM 6340F). Gold top electrodes with a diameter of 0.6 mm were deposited onto the surface using lift-off processing and E-beam evaporation for electrical measurement. Impedance spectroscopy from 100 Hz to 1 MHz was measured with the temperature ranging from 25 to 275 °C by an Agilent 4294A precision impedance analyzer at the ac oscillation level of 500 mV. Each measured temperature was kept constant with an accuracy of ±1 °C. The ac conductivity of the composite thick films was estimated from the standard relation:

$$\sigma_{AC} = \omega\varepsilon'\varepsilon_0 \tan\delta \quad (1)$$

where ε_0 and ε' are the permittivity of the free space and real part of measured dielectric permittivity, ω is the angular frequency and $\tan\delta$ is the loss tangent.

3. Results and discussion

XRD pattern of the multiferroic CFO–PZT composite thick film shows a pure PZT perovskite phase, as can be seen in Fig. 1, which is similar to previous result [16]. The absence of CFO spinel phase can be attributed to its deeply buried distribution in the PZT matrix. The scanning electron microscopic pictures of the composite thick film are exhibited in Fig. 2. The optimized thick films densification by sufficient sol infiltration is shown clearly in Fig. 2(a) along with a uniform surface morphology. Fig. 2(b) shows a cross-sectional picture of the composite thick film, where the film thickness is estimated as 5.7 μm. Compared with our initial attempts on multiferroic thick films [15], the present thick film quality shows a significant improvement.

Fig. 3 shows the frequency and temperature dependent real and imaginary part of impedance (Z' and Z'', respectively). Fig. 3(a) shows that the Z' values decrease with increasing frequency and a weak relaxation peak (marked with arrows) is observed initially at 25 °C. Furthermore, this relaxation peak moves to high frequency side with increasing temperature and finally disappears beyond 125 °C. This corresponds to the faint relaxation behavior of Z'' observed in Fig. 3(b) (marked with arrows), where the imaginary impedance decreases with increasing frequency in an approximately linear manner below 225 °C due to the high sample resistance. Only once the temperature reaches 275 °C, do we observe a smoothing of the relaxation peak into the measured window from low frequency, as exhibited in Fig. 3(b). The relaxation corresponds to another relaxation indicated in Fig. 3(a) under a similar frequency range. According to the Arrhenius law below [18],

$$fr = f_1' \exp\left[-\frac{Er}{k_B T}\right], \quad (2)$$

where f_1' is the relaxation frequency at an infinite temperature and Er the activation energy for the dielectric relaxation, the activation energy is estimated as 0.58 eV. In addition, it is noted that the Z'' values are slightly reduced with increasing temperature, indicating a weak sensing behavior of dc conductivity to temperature. This is similar to the situation of the multilayered PZT/CFO thin film below 500 K [14].

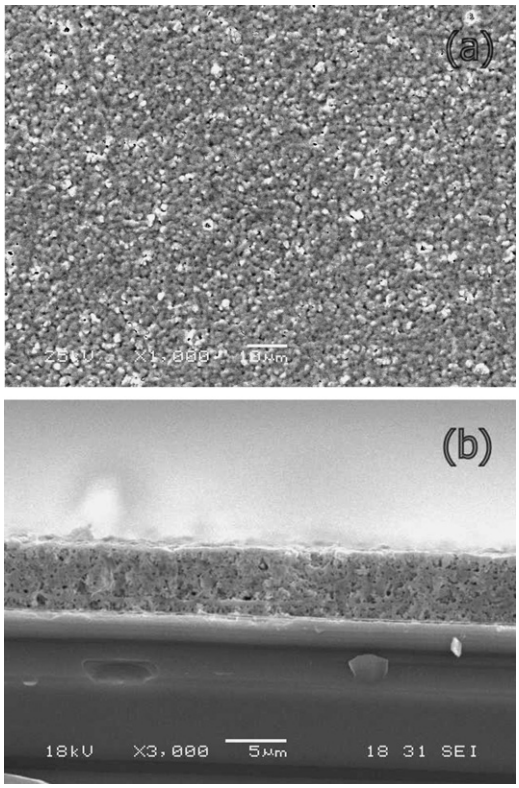

Fig. 2. Surface morphology (a) and cross-sectional picture (b) of the CFO–PZT composite thick film.

Nyquist (or Cole–Cole) plots of impedance data at different temperatures are shown in Fig. 4. At room temperature two poorly resolved semicircle arcs are observed: a small arc at high frequency (inset) which is largely obscured by a larger semicircular arc at low frequency. From 25 to 225 °C, both semicircular arcs exist; but when the temperature reaches 275 °C, only a single broad semicircle is observed in the low frequency region without additional contribution detected in the high frequency region. This is because the time constant at high frequency is decreased with increasing temperature, leading to a loss of resolution obscuring the semicircle in the impedance plot at high temperature [19]. Semicircles size in impedance plots is scaled according to the magnitude of their resistance, where two responses often have greatly differing magnitudes of R (often by orders of magnitude), the larger resistive response dominates entirely, making the resolution of the smaller resistive response difficult. In such cases electric modulus data, where semicircles scale inversely to capacitance, are often useful for resolving the different relaxations [20]. The electric modulus (M^*) is calculated from the following equation:

$$M^* = M' + jM'' = j\omega C_0 Z^* = j\omega C_0 (Z' - jZ'') \quad (3)$$

where M' and M'' are real and imaginary part of electric modulus, $C_0 = \varepsilon_0 A/d$ is the vacuum capacitance of the measuring cell and electrodes with an air gap of the sample thickness, ε_0 is the permittivity of free space, A and d are cross-sectional area of the electrode deposited on the sample and film thickness, and ω is the angular frequency.

From the values of M^*, the values of M' and M'' were calculated using the relation $M' = \omega C_0 Z''$ and $M'' = \omega C_0 Z'$. Furthermore, the values of M' and M'' were plotted as shown in Fig. 5(a), where

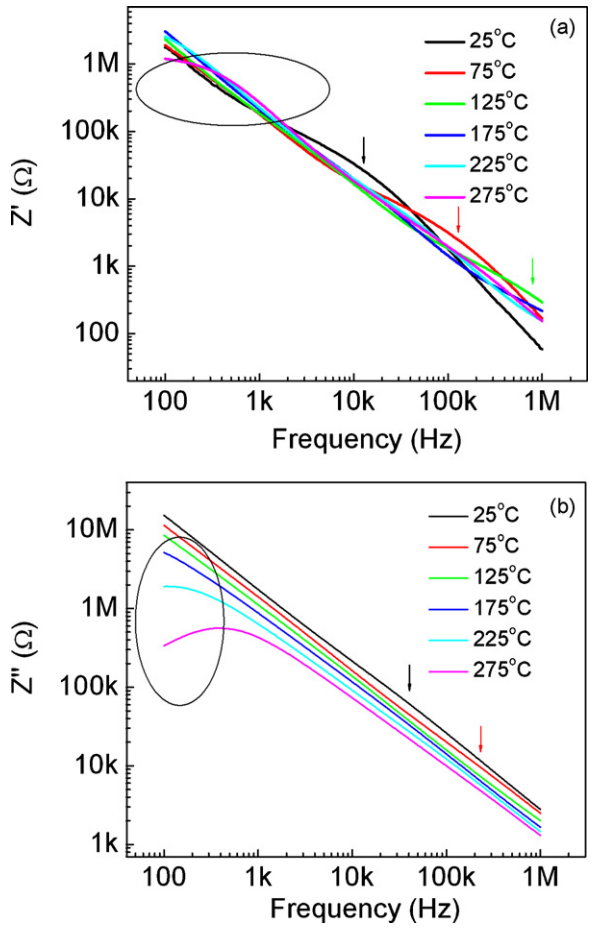

Fig. 3. Temperature and frequency dependent real (a) and imaginary impedance spectra (b) of CFO–PZT composite thick film.

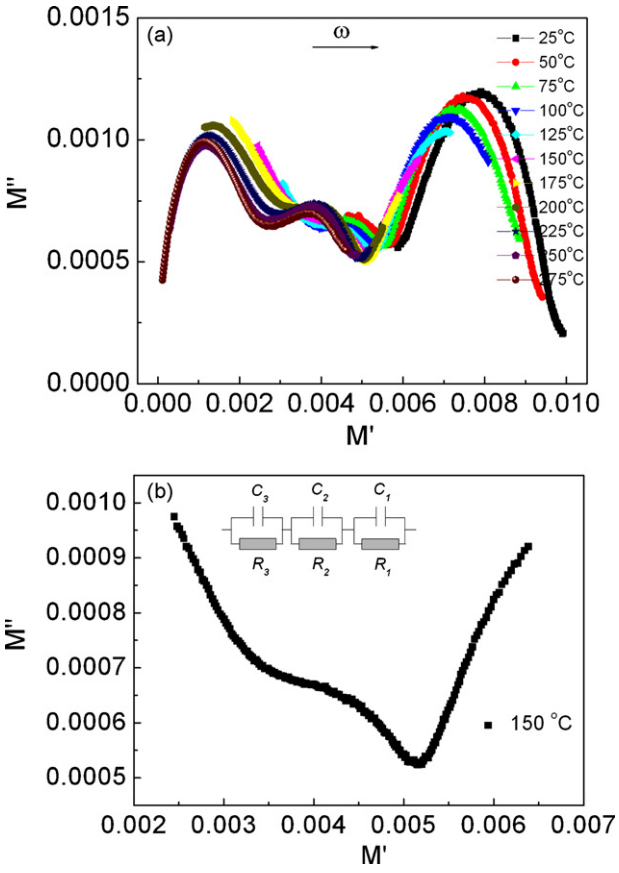

Fig. 5. Temperature and frequency dependent M''–M' of CFO–PZT composite thick film (a); the typical one at 150 °C (b); and the inset in (b) corresponds to the equivalent electric circuit.

the direction of increasing frequency was also indicated. Two very large semicircle arcs are observed separately below 125 °C and above 200 °C. A small semicircle arc is also observed over the whole temperature range. The low temperature large semicircle arc is induced by grain effect, while the high temperature arc can be attributed to the grain boundary effect. It is noted that the magnitudes of the grain boundary capacitance are comparable to the grain capacitance. This is due to the heterogeneous composite structure, which is also demonstrated in thickness dependent PZT/CFO multilayered thin films [14]. Additionally, when the temperature is increased beyond 125 °C, the grain effect has moved out of the frequency window; but the grain boundary effect has not entered into this window until 200 °C. In this temperature range of 125–200 °C, it can be seen from Fig. 5(b) that three effects are observed at 150 °C. Besides the high frequency degraded grain effect and the low frequency strengthened grain boundary effect, there is another effect in between them, this phenomenon was not found in PZT/CFO thin films [14]. Actually, these three effects are consistent with an equivalent circuit comprising three parallel *RC* elements, as shown in the inset in Fig. 5(b). Here, the low frequency arc corresponds to the R_3C_3 response and the high frequency arc corresponds to the R_1C_1 response. Both responses result from high frequency grain effect and low frequency grain boundary effect, respectively. R_2C_2 response corresponds to the effect observed at intermediate frequency range at 150 °C. Furthermore, this effect is gradually strengthened with increasing temperature, evident in Fig. 5(a). Possible cause for this effect is due to an additional grain boundary effect. The composite thick film samples were designed as a sandwich structure, the central layer is CFO–PZT heterogeneous composite layer, while its top and bottom sides are constituted by pure PZT homogeneous composite layer. This will make the composite thick film produce two different grain boundary effects. Moreover, due to the low ratio of CFO–PZT layer in this composite design, the weaker R_2C_2 response should be attributed to the grain boundary effect between CFO and PZT grains. For clarity, the value of C_2 can be extracted from the semicircular arc intercepts on the M' axis in Fig. 5(b), C_2 and f_{max} data are used to calculate R_2 using

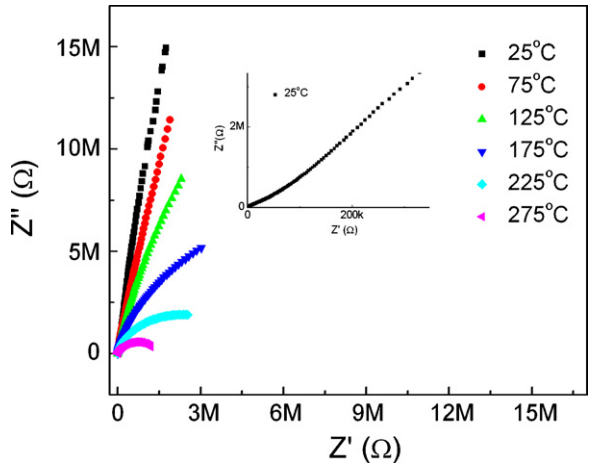

Fig. 4. Nyquist plots of impedance data of CFO–PZT composite thick film at selected temperatures; inset one is the typical plot at 25 °C.

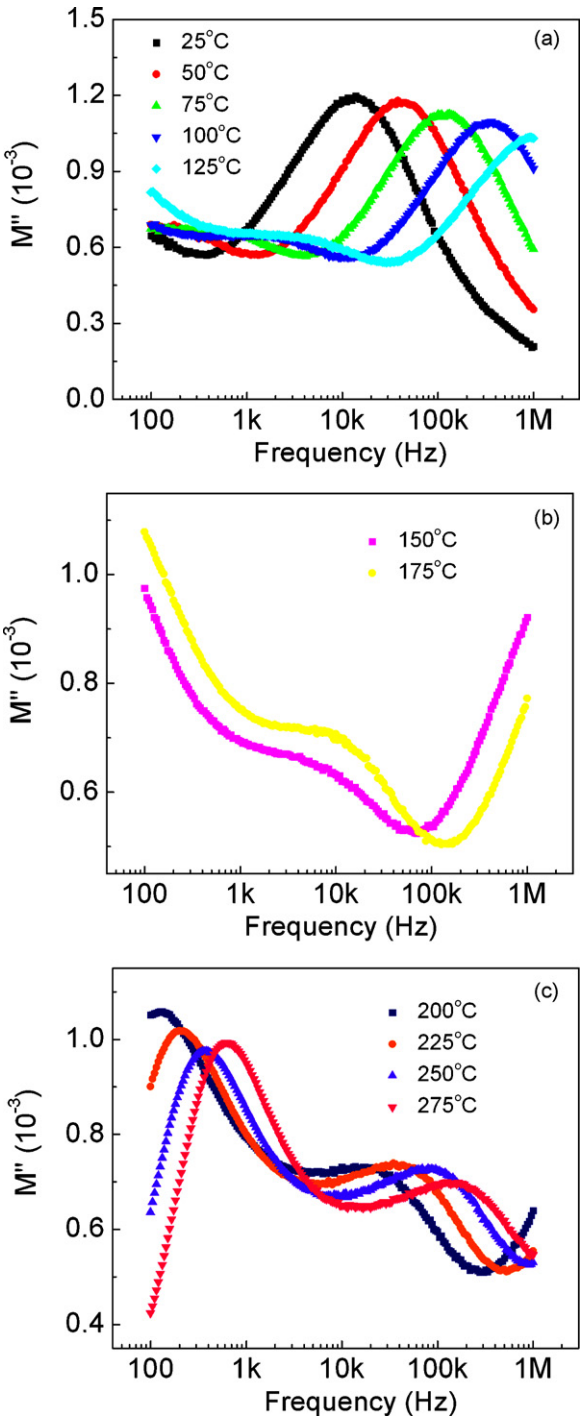

Fig. 6. Temperature dependent imaginary electric modulus spectral of CFO–PZT composite thick film from 25 to 125 °C (a); 150 to 175 °C (b); and 200 to 275 °C (c).

Eq. (4),

$$\omega\tau = 2\pi f_{max} RC = 1, \quad (4)$$

where f_{max} is the frequency of maxima of semicircles and τ is the relaxation time. The calculated C_1 and R_1 are 142 pF and 295 kΩ, respectively. At 150 °C, it is not possible to calculate R_1 and R_3 exactly in the same manner as f_{max} for the semicircular arc corresponding to R_2C_2 as their maximum frequencies are beyond the measurable frequency range.

Fig. 6 presents the frequency dependence of imaginary electric modulus at all temperatures. It can be seen from Fig. 6(a) that a well defined relaxation peak appears in the temperature range of 25–125 °C. Meanwhile, a step-like behavior is also observed at low frequency side, which should be attributed to the CFO–PZT grain boundary effect due to the low resistivity of the CFO phase [21], leading to its easier to be thermal activated than insulated PZT phase. Furthermore, the relaxation peak and this step-like behavior are moving to the high frequency side with increasing temperature. When the temperature reaches 150 °C, the relaxation peak that appeared on high frequency side has completely degraded and only its left wing is observed at this temperature, as can be seen in Fig. 6(b). Furthermore, the step-like behavior is gradually forming into another peak with further increasing temperature, as can be seen in Fig. 6(c), where this step-like behavior has totally formed into a very broad relaxation peak. Moreover, the third relaxation peak, which is even narrower than the first relaxation peak observed below 125 °C, is moving into the frequency window from low frequency side with further increasing temperature. From the evolving process of these relaxation behaviors, we can see three responses in electric modulus spectra which are consistent with the observations in Fig. 5. From 25 to 125 °C, the first two responses coexist: one is corresponding to the relaxation peak at high frequency side, the other is reflected by the step-like relaxation behavior. During 150–175 °C, the step-like relaxation behavior is dominant. Above 175 °C, another narrow low frequency relaxation peak predominates in the frequency window along with a strengthened step-like behavior at high frequency side. Both relaxation peaks mentioned (not the step-like) are actually corresponding to the two weak relaxation behaviors in impedance spectra (Fig. 3). This is similar to the situation of PZT/CFO multilayered thin films [14], where a broad relaxation peak appeared at lower temperature and higher frequency and another narrow relaxation peak observed at higher temperature and lower frequency in modulus spectra, grain effect and grain boundary effect are attributed to them, respectively. However, the step-like behavior communicating both relaxation peaks is ignored in this literature [14], which is consistent with the observations of Fig. 5. Heterogeneous CFO–PZT grain boundary effect is attributed to it. From the three features in Fig. 6, we can also calculate their activation energies in terms of Arrhenius law. The one calculated from the peaks in Fig. 6(a) is 0.43 eV; while the calculated values from the two kinds of peaks in Fig. 6(c) are 0.47 and 0.65 eV, which are corresponding to the high frequency range and low frequency range, respectively. Compared with the activation energy of 0.58 eV estimated from high temperature impedance relaxation in Fig. 3, both values of 0.47 and 0.65 eV from two kinds of grain boundaries effects in modulus spectra should be co-contributed to this average effect. While the other activation energy of 0.43 eV calculated from modulus spectra, is contributed from the grain effect, which is not expressed clearly in impedance spectra. Both activation energy values from grain effect and average grain boundary effect is comparable with the values of three-layer PZT/CFO thin films, where 0.4187 and 0.5684 eV were reported [14]. This is also confirming the present work, where the grain boundary effect is further extended.

Real and imaginary dielectric constants (ε' and ε'') are plotted against the frequency at all temperatures, as shown in Fig. 7. It can be seen from Fig. 7(a) that real dielectric constant is increasing with temperature but decreasing with frequency. For example, at 1 MHz, the ε' value is increased from 215 to 455 when the temperature is promoted from 25 to 275 °C, while at 100 Hz, the ε' value is increased dramatically from 385 to 1349 under the same temperature range. This indicates a strong low frequency dispersion phenomenon in the real dielectric constant. In addition, a dielectric relaxation behavior is observed at high frequencies but below 150 °C. The plots of the imaginary part of dielectric constant versus frequency are shown in Fig. 7(b) for temperatures from 25 to 150 °C and Fig. 7(c) for temperatures from 175 to 275 °C. A peak is observed

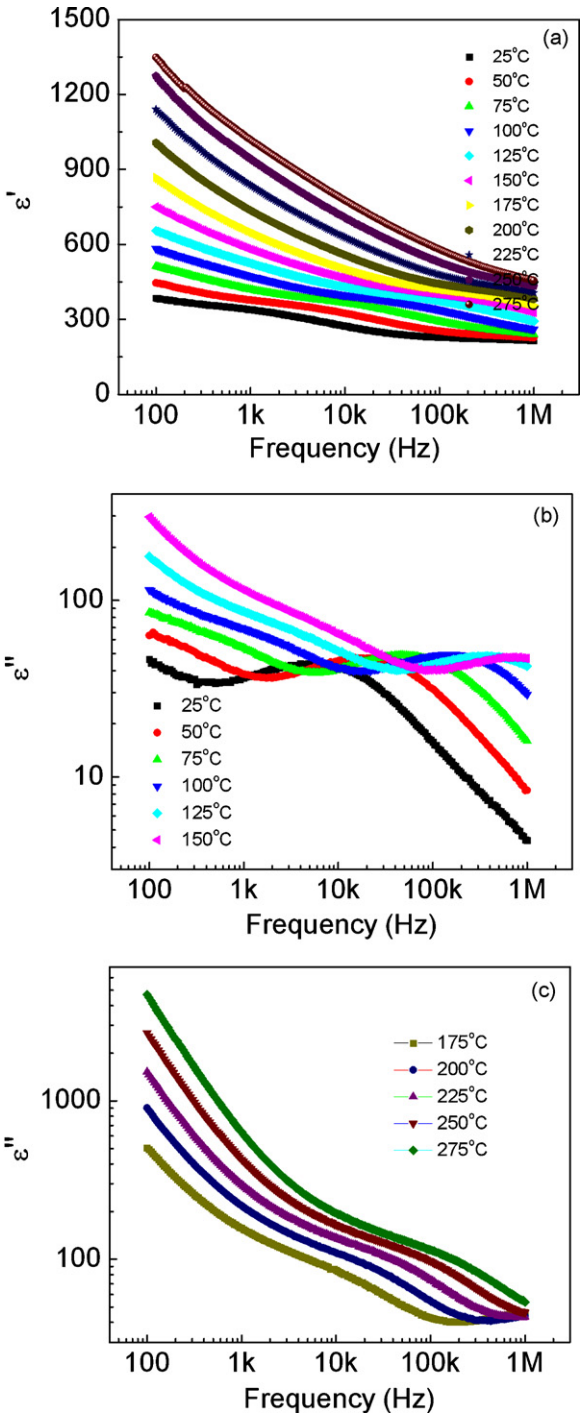

Fig. 7. Temperature and frequency dependent real dielectric permittivity (ε') of CFO–PZT composite thick film (a) and its dependent imaginary dielectric permittivity (ε'') from 25 to 150 °C (b); and 175 to 275 °C (c).

in ε'' versus frequency plots at and below 150 °C (Fig. 7(b)), which correspond to the relaxation behavior in ε' curve. Above 175 °C, no peak in ε'' curve is observed in the measurable frequency range but several features are exhibited in Fig. 7(c). First, the slop of the straight line of log–log plot at low frequency side equals −1, which is the natural result of the frequency independent conduction [22]. Second, a nearly constant loss region at intermediate frequencies indicates an increasing conductivity with frequency due to Eq. (1). Third, another nearly constant loss region at the high frequency side is indicative of another increasing conductivity region.

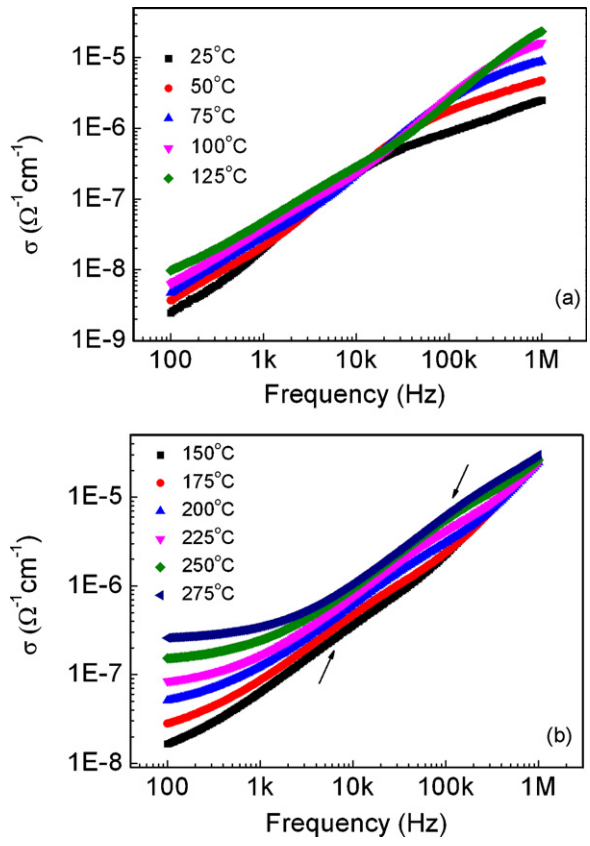

Fig. 8. Temperature dependent ac conductivity spectra (σ') of CFO–PZT composite thick film from 25 to 150 °C (a) and 175 to 275 °C (b).

Fig. 8 shows the ac conductivity curves of CFO–PZT composite thick film as a function of frequency at different temperatures. It can be seen from Fig. 8 that conductivity value is increasing with frequency. Take the minimum and maximum measured temperature as examples. With increasing frequency from 100 Hz to 1 MHz, the conductivity values are increasing from 2.5×10^{-9} and 2.6×10^{-7} to 2.5×10^{-6} and $3.0 \times 10^{-5}\ \Omega^{-1}\ \mathrm{cm}^{-1}$ at 25 and 275 °C, respectively. This belongs to a normal thermal mechanism. These conductivity values are slightly less than those of the multilayered PZT/CFO films [14], indicating a high quality of the present composite thick films.

Fig. 8(a) shows two features at and below 125 °C. First, there is a strong rise at low frequencies. This is the grain boundary blocking effect. Second, the conductivity does not increase rapidly at high frequencies, but shows a temperature dependent dispersion behavior. This is corresponding to the dielectric relaxation in Fig. 7, which is ascribed to the bulk conductivity relaxation. The σ in the second feature can be described by "universal dielectric response" (UDR) [23].

$$\sigma = \sigma_{\mathrm{dc}} + \sigma_0 f^s \tag{5}$$

where σ_{dc} is the dc bulk conductivity, σ_0 is a constant, f is the frequency, and exponent s is smaller than 1. Eq. (5) is a common feature for most disordered systems and amorphous semiconductors [23]. It is typical of thermal assisted tunneling between localized states. In our system, it may be ascribed to the polaron relaxation [18], where ion hopping is restricted by the low temperature and high frequency, which cannot provide the ions with enough high energy or available time to hop out of their sites, resulting in the ions vibrate in their own sites iteratively.

Fig. 8(b) shows three features for the conductivity spectra at and above 150 °C. The first one is that low frequency conductivity curves tend to flatten with further increasing temperature, suggesting

the dc conductivity behavior. It is clearly seen that this frequency independent conductivity becomes strengthened with increasing temperature, which is consistent with the low frequency slop in dielectric spectra (Fig. 7(c)). The second one is a weak conductivity relaxation appeared at intermediate frequency range (marked as two arrows), which is moving to high frequency side with increasing temperature. The third one is that the conductivity curves at high frequency side are merging together but also show a linearly increase at each temperature. The whole conductivity curve is similar to that of PZT/CFO multilayered thin films below 500 K [14], but much attention has been paid to the conductivity behavior above 500 K in this literature. For our CFO–PZT composite thick film, the jump relaxation model [24] can explain its conductivity characteristics. The frequency independent plateau at low frequencies is attributed to the long-range translational motion of ions. According to this model, the conductivity at the low frequency region is associated with successful hops to its neighborhood vacant site due to the available long time period. It is reasonable that such successive jumps can result in a long-range translational motion of ions, finally contributing to dc conductivity. Above the intermediate frequency (>5 kHz), two competing relaxation processes may be visualized: (1) the jumping ion to jump back to its initial position, i.e., unsuccessful hopping and (2) the neighborhood ions become relaxed with respect to the ion's position, successful hopping. The increase in the ratio of successful to unsuccessful hopping with increasing temperature leads to the relaxation behavior at intermediate frequency due to sufficient time for ion successful hopping. Unfortunately for the high frequency conductivity behavior, the time is insufficient for most of ions to hop from their own sites, its conductivity mechanism should be attributed to the vibrational relaxation caused by anharmonicity [25], where unsuccessfully ions jumps should be responsible. When the temperature is increased from 150 to 275 °C, we can see the slope of conductivity curve is gradually decreasing, indicative of a thermal mechanism, from which more thermal energy is supplied in order that most of ions can have a successful hopping.

4. Conclusions

Multiferroic $CoFe_2O_4$–$Pb(Zr_{0.53}Ti_{0.47})O_3$ composite thick films have been fabricated onto $Pt/TiO_2/SiO_2/Si$ substrate. Film densification and crystallization have been optimized by sufficient sol infiltration and 800 °C annealing temperature. X-ray diffraction shows a pure PZT perovskite phase and the absence of CFO phase is attributed to the deep distribution of CFO particles in the central part of the composite thick film. Scanning electron microscope exhibits a uniform surface and sharp cross-sectional morphology with 5.7 μm of thickness. Impedance spectroscopy and electric modulus analysis indicate the contributions from grain and grain boundary effect at different frequencies and temperatures, resulting in two different grain boundary effects being observed in modulus spectra. Activation energy calculated from two methods keep in good agreement with each other. Dielectric spectra reveal a polaron relaxation below 150 °C and above this temperature, dc conductivity region and two nearly constant loss regions are indicated, which is also demonstrated in ac conductivity spectra. Furthermore, ion hopping and transport are also revealed by ac conductivity analysis, jump relaxation mode is well used to clarify them.

Acknowledgement

This work was supported by research grant RCA-08/018 funded by Singapore National Research Foundation.

References

[1] J. Liu, M.Y. Li, L. Pei, J. Wang, B.F. Yu, X. Wang, X.Z. Zhao, J. Alloys Compd. 453 (2010) 544–548.
[2] L.H. Pang, W.J. Ji, Y. Zhang, L. Wang, S.T. Zhang, Z.L. Luo, Y.F. Chen, J. Phys. D 42 (2009) 045304–045305.
[3] Y. Zhou, J.C. Zhang, L. Li, Y.L. Su, J.R. Cheng, S.X. Cao, J. Alloys Compd. 484 (2009) 535–539.
[4] W. Chen, S. Shannigrahi, X.F. Chen, Z.H. Wang, W. Zhu, O.K. Tan, Solid State Commun. 150 (2010) 271–274.
[5] C.W. Nan, M.I. Bichurin, S.X. Dong, D. Viehland, G. Srinivasan, J. Appl. Phys. 103 (2008) 031101–031135.
[6] Y.J. Wu, L.H. Tang, H.L. Li, X.M. Chen, J. Alloys Compd. 496 (2010) 269–272.
[7] L. Zhu, Y.L. Dong, X.H. Zhang, Y.Y. Yao, W.J. Weng, G.R. Han, N. Ma, P.Y. Du, J. Alloys Compd. 503 (2010) 426–430.
[8] W. Chen, Z.H. Wang, W. Zhu, O.K. Tan, J. Phys. D 42 (2009) 075421–075425.
[9] L.H. Yin, Y.P. Sun, F.H. Zhang, W.B. Wu, X. Luo, X.B. Zhu, Z.R. Yang, J.M. Dai, W.H. Song, R.L. Zhang, J. Alloys Compd. 488 (2009) 254–259.
[10] H.L. Zhang, X.M. Chen, T. Wang, F.F. Wang, W.Z. Shi, J. Alloys Compd. 500 (2010) 46–48.
[11] M. Liu, X. Li, J. Lou, S.J. Zheng, K. Du, N.X. Sun, J. Appl. Phys. 102 (2007) 083911–083913.
[12] H.C. He, J. Ma, J. Wang, C.W. Nan, J. Appl. Phys. 103 (2008) 034103–034105.
[13] A.S. Fawzi, A.D. Sheikh, V.L. Mathe, J. Alloys Compd. 493 (2010) 601–608.
[14] N. Ortega, A. Kumar, P. Bhattacharya, S.B. Majumder, R.S. Katiyar, Phys. Rev. B 77 (2008) 014111–014210.
[15] W. Chen, Z.H. Wang, C. Ke, W. Zhu, O.K. Tan, Mater. Sci. Eng. B 162 (2009) 47–52.
[16] W. Chen, W.G. Zhu, X.F. Chen, Z.H. Wang, J. Am. Ceram. Soc. 93 (2010) 796–799.
[17] Z.H. Wang, J.M. Miao, W.G. Zhu, J. Eur. Ceram. Soc. 27 (2007) 3759–3764.
[18] L. Zhang, Z.J. Tang, Phys. Rev. B 70 (2004) 174306–174316.
[19] A. Srivastava, A. Garg, F.D. Morrison, J. Appl. Phys. 105 (2009) 054103–054106.
[20] F.D. Morrison, D.C. Sinclair, A.R. West, J. Am. Ceram. Soc. 84 (2001) 531–538.
[21] I.H. Gul, A. Maqsood, J. Alloys Compd. 465 (2008) 227–231.
[22] X. Chen, A.I. Kingon, O. Auciello, Proceedings of Eighth IEEE International Symposium on Applications of Ferroelectrics, Greenville, SC, USA, 1992, p. 229.
[23] S.R. Elliott, Adv. Phys. 36 (1987) 135–218.
[24] A.K. Jonscher, Nature 267 (1977) 673–679.
[25] C. Leon, A. Rivera, A. Varez, J. Sanz, J. Santamaria, Phys. Rev. Lett. 86 (2001) 1279–1282.